



Article

2-Acetamido-2-deoxy-D-glucono-1,5-lactone Sulfonylhydrazones: Synthesis and Evaluation as Inhibitors of Human OGA and HexB Enzymes

Mariann Kiss ¹, István Timári ¹, Teréz Barna ², Zuzana Mészáros ^{3,4}, Kristýna Slámová ³, Pavla Bojarová ³, Vladimír Křen ³, Joseph M. Hayes ⁵ and László Somsák ^{1,*}

¹ Department of Organic Chemistry, University of Debrecen, POB 400, H-4002 Debrecen, Hungary; kiss.mariann@science.unideb.hu (M.K.); timari.istvan@science.unideb.hu (I.T.)

² Department of Genetics and Applied Microbiology, University of Debrecen, POB 400, H-4002 Debrecen, Hungary; barna.terez@science.unideb.hu

³ Laboratory of Biotransformation, Institute of Microbiology of the Czech Academy of Sciences, Vídeňská 1083, CZ-14220 Praha 4, Czech Republic; zuzana.meszáros@biomed.cas.cz (Z.M.); slamova@biomed.cas.cz (K.S.); bojarova@biomed.cas.cz (P.B.); kren@biomed.cas.cz (V.K.)

⁴ Faculty of Food and Biochemical Technology, University of Chemistry and Technology Prague, Technická 1903/3, CZ-16628 Praha 6, Czech Republic

⁵ School of Pharmacy & Biomedical Sciences, University of Central Lancashire, Preston PR1 2HE, UK; JHayes@uclan.ac.uk

* Correspondence: somsak.laszlo@science.unideb.hu

Abstract: Inhibition of the human *O*-linked β -*N*-acetylglucosaminidase (hOGA, GH84) enzyme is pharmacologically relevant in several diseases such as neurodegenerative and cardiovascular disorders, type 2 diabetes, and cancer. Human lysosomal hexosaminidases (hHexA and hHexB, GH20) are mechanistically related enzymes; therefore, selective inhibition of these enzymes is crucial in terms of potential applications. In order to extend the structure–activity relationships of OGA inhibitors, a series of 2-acetamido-2-deoxy-D-glucono-1,5-lactone sulfonylhydrazones was prepared from D-glucosamine. The synthetic sequence involved condensation of *N*-acetyl-3,4,6-tri-*O*-acetyl-D-glucosamine with arenesulfonylhydrazines, followed by MnO₂ oxidation to the corresponding glucono-1,5-lactone sulfonylhydrazones. Removal of the *O*-acetyl protecting groups by NH₃/MeOH furnished the test compounds. Evaluation of these compounds by enzyme kinetic methods against hOGA and hHexB revealed potent nanomolar competitive inhibition of both enzymes, with no significant selectivity towards either. The most efficient inhibitor of hOGA was 2-acetamido-2-deoxy-D-glucono-1,5-lactone 1-naphthalenesulfonylhydrazone (**5f**, $K_i = 27$ nM). This compound had a K_i of 6.8 nM towards hHexB. To assess the binding mode of these inhibitors to hOGA, computational studies (Prime protein–ligand refinement and QM/MM optimizations) were performed, which suggested the binding preference of the glucono-1,5-lactone sulfonylhydrazones in an *s-cis* conformation for all test compounds.

Keywords: hOGA; hHexB; inhibitor; glyconolactone sulfonylhydrazone; Prime refinement; QM/MM optimization

Citation: Kiss, M.; Timári, I.; Barna, T.; Mészáros, Z.; Slámová, K.; Bojarová, P.; Křen, V.; Hayes, J.M.; Somsák, L. 2-Acetamido-2-deoxy-D-glucono-1,5-lactone Sulfonylhydrazones: Synthesis and Evaluation as Inhibitors of Human OGA and HexB Enzymes. *Int. J. Mol. Sci.* **2022**, *23*, 1037. <https://doi.org/10.3390/ijms23031037>

Academic Editor: Claudio O. Gualerzi

Received: 15 December 2021

Accepted: 15 January 2022

Published: 18 January 2022

Publisher's Note: MDPI stays neutral with regard to jurisdictional claims in published maps and institutional affiliations.



Copyright: © 2022 by the authors. Licensee MDPI, Basel, Switzerland. This article is an open access article distributed under the terms and conditions of the Creative Commons Attribution (CC BY) license (<https://creativecommons.org/licenses/by/4.0/>).

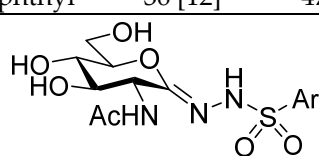
1. Introduction

O-GlcNAcylation is a dynamic posttranslational modification in which a single β -*N*-acetylglucosamine (GlcNAc) moiety is added to or removed from the serine/threonine residues of nucleocytosolic and mitochondrial proteins. The dynamic cycling of *O*-GlcNAc modification on numerous, functionally distinct proteins is catalyzed by two enzymes: *O*-linked β -*N*-acetylglucosaminyltransferase (OGT, EC 2.4.1.255; GT41) and β -*N*-

acetylglucosaminidase (OGA, EC 3.2.1.169; GH84) in response to cellular signals or cellular phases, similar to phosphorylation [1]. Indeed, in many cases, phosphorylation and O-GlcNAcylation target the same serine/threonine residues. Misregulation of the O-GlcNAc cycle can influence numerous cell signaling processes and contribute to the development of various diseases such as neurodegenerative and cardiovascular disorders, type 2 diabetes, and cancer [2]. Changes in the O-GlcNAcylation status of proteins can lead to alterations in protein folding, cellular localization, and catalytic activity [3], all of which can actively influence downstream biological processes associated with the protein in question and play a critical role in the development and progression of chronic diseases. Numerous papers [4–7] demonstrated that inhibition of OGA reduces the amount of the pathological tau protein in the brain, most likely by increasing its O-GlcNAcylation. Thus, by decreasing its phosphorylation, tau remains in the soluble, non-toxic form with reduced aggregation. Therefore, the development of OGA inhibitors has considerable significance in the design of new potential treatments for Alzheimer's disease and other neurodegenerative tauopathies, which belong to the most serious health and socio-economic challenges of modern society.

PUGNAc (Table 1, I) was one of the first inhibitors of OGA [8]; however, it is not selective, since it also inhibits lysosomal hexosaminidases (HexA and HexB, EC 3.2.1.52; GH20) that cleave GlcNAc and GalNAc residues from oligosaccharides and glycosphingolipids. Neither the activity nor the selectivity of PUGNAc was significantly altered by modifications of the aromatic moiety [9]. OGA is active at neutral pH and is specific for the GlcNAc substrate, while hexosaminidases act at acidic (lysosomal) pH and show an affinity also for GalNAc. Both OGA and HexA/HexB utilize the substrate-assisted catalytic mechanism, in which the 2-acetamido group of the substrate forms an oxazoline intermediate [10], although they do not share sequence similarity. The synthesis of selective inhibitors can help avoid side effects by simultaneous inhibition of both enzymes. Any non-specific inhibition of hexosaminidases may lead to lysosomal ganglioside accumulation, resulting in the neurodegenerative Tay-Sachs and Sandhoff diseases [11].

Table 1. Selected inhibitors of OGA with their activity against HexA/B enzymes and the target compounds of this study.

I			II		
Ar	K _i (nM)		Ar	K _i (nM)	
	OGA	HexB		OGA	HexA/B ^a
Ph (PUGNAc)	46 [10]	36 [10]	Ph	190 [12]	205 [12]
4-Me-C ₆ H ₄ -	28 [9]	21 [9]	4-Me-C ₆ H ₄ -	155 [12]	332 [12]
4-Br-C ₆ H ₄ -	56 [9]	47 [9]	4-Cl-C ₆ H ₄ -	83 [12]	170 [12]
			2-Naphthyl	36 [12]	47 [12]
Target compounds					

^a This enzyme contains two predominant isozymes, Hex A, a heterodimer, and Hex B, a homodimer.

In our previous work [12], 2-acetamido-2-deoxy-D-gluco-1,5-lactone 4-arylsemi-carbazones (Table 1, II) were found to be nanomolar inhibitors of both hOGA and HexA/HexB enzymes. Nevertheless, these inhibitors showed only moderate selectivity

($K_{i(\text{Hex})}/K_{i(\text{OGA})} = 1\text{--}2$). This was the first study in which modifications were made to the urethane linking moiety between the glycone and the aromatic residue related to PUGNAc. In the present work, our aim was to make a structure–affinity relationship study of the said linker to determine how respective modifications affect the inhibition of OGA and the selectivity towards HexA/HexB. For this purpose, a library of 2-acetamido-2-deoxy-D-glucono-1,5-lactone arenesulfonylhydrazones (Table 1, target compounds) was prepared and studied as inhibitors of the above enzymes using kinetic and computational methods.

2. Results and Discussion

2.1. Synthesis of Inhibitors

Although some glycono-1,5-lactone tosylhydrazones are known in the literature [13–15], no analogous derivatives of 2-acetamido-2-deoxy-D-glucono-1,5-lactone could be found. Therefore, the synthesis of the planned inhibitors (Table 2) was based on our previous work [12] encompassing the synthesis of 2-acetamido-2-deoxy-D-glucono-1,5-lactone semicarbazones. The starting material 2-acetamido-3,4,6-tri-*O*-acetyl-2-deoxy-D-glucopyranose (**1**) was obtained from D-glucosamine hydrochloride by a well-known two-step procedure [16,17] in 83% overall yield. Compound **1** was then converted by arenesulfonyl hydrazides **2** (either commercial or obtained from the corresponding arenesulfonyl chloride as described in the literature [18]) in the presence of 10 mol% *p*-toluenesulfonic acid catalyst in chloroform to afford *N*-glycosyl arenesulfonyl hydrazides **3**. The oxidation reactions to yield lactone hydrazones **4** were carried out with activated MnO_2 in dichloromethane at reflux temperature. *O*-Deprotection of **4** was performed with a solution of NH_3 in MeOH to result in test compounds **5**. The overall yields of these five-step synthetic sequences affording inhibitors **5** from D-glucosamine were in the range of 26–44%.

Table 2. Synthesis of test compounds **5**.

Reagents and conditions:
 (a) $\text{ArSO}_2\text{NHNH}_2$ (**2**, 1.5 equiv.), *p*-TsOH·H₂O (0.1 equiv.), CHCl_3 , reflux; (b) activated MnO_2 , abs. CH_2Cl_2 , reflux; (c) NH_3/MeOH , r.t.

	Ar	Products and yields (%)			Overall yield of 5 from D-glucosamine
		3	4	5	
a	<i>p</i> -MePh	77	69	94	41
b	<i>p</i> -CF ₃ Ph	85	60	83	35
c	<i>p</i> -FPh	86	72	85	44
d	<i>p</i> -ClPh	89	77	78	44
e	2-naphthyl	76	56	75	26
f	1-naphthyl	89	66	80	39

To determine the configuration of the C=N bond in compounds **5**, a nuclear Overhauser effect (NOE)-based NMR approach was applied to **5d**. A 2D ^1H - ^1H EASY ROESY experiment [19] was performed, which is a robust variant of NOE methods for small- and medium-sized molecules. The maximum spatial distance that can provide an NOE signal is about 5 Å. Thus, the *E*-*Z* isomeric forms of compound **5d** are expected to be distinguished based on informative NOE cross-peaks between the N(2)H and characteristic protons of the carbohydrate unit. In the ^1H - ^1H ROESY spectrum (Figure S1) obtained for compound **5d**, NOE cross-peaks between the N(2)H resonance and H(5'), H(6'a,b) resonances can be observed (Figure 1), which indicate the vicinity in space of these protons and so the existence of the *Z* isomeric form. Since both the ^1H and ^{13}C NMR spectra for the other compounds **5** closely resemble those of **5d**, one can safely conclude the presence of the *Z* isomer also in those derivatives.

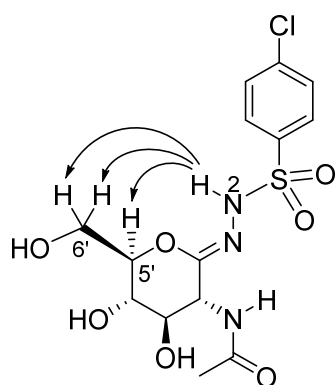


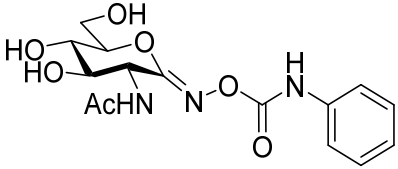
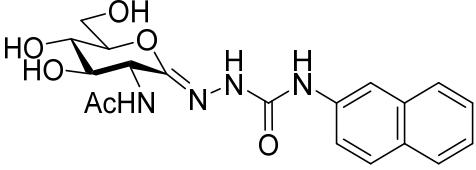
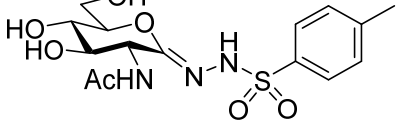
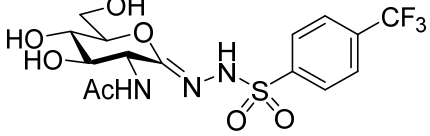
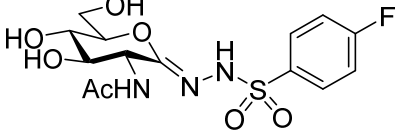
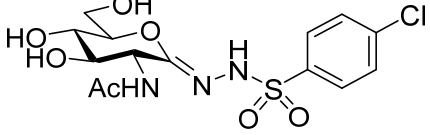
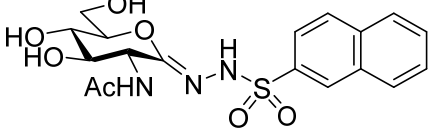
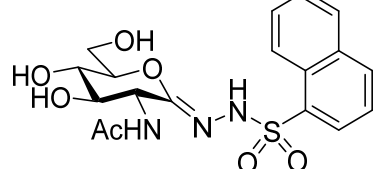
Figure 1. Nuclear Overhauser effects (NOEs) observed in compound **5d**.

2.2. Inhibition of hOGA and hHexB by 2-Acetamido-2-deoxy-D-glucono-1,5-lactone Arenesulfonylhydrazones

The inhibitory potency of compounds **5a–f** was evaluated against recombinant hOGA and hHexB enzymes. The enzymes were prepared and purified as described previously [12,20]. For inhibition of hOGA, fluorescent 4-MU-GlcNAc was used as the substrate. Inhibition constants (K_i) were determined by linear regression of data from Dixon plots using the competitive model as this mode of inhibition was proved by the Cornish-Bowden plots. In the case of inhibition of hHexB, Michaelis–Menten kinetics were evaluated using *p*NP-GlcNAc as a colorimetric substrate. Inhibition constants (K_i) were determined by nonlinear regression analyses by employing the competitive inhibition model (cf. the Experimental section and Supplementary Materials).

The inhibition constants (K_i) for most inhibitors **5** against hOGA were in the low nanomolar range (Table 3). The most potent inhibitors of hOGA were sulfonylhydrazones **5e** and **5f**, while **5b** proved to be the weakest one. On the other hand, lower K_i values against hHexB were obtained for all but one of the compounds, indicating that compounds **5** are better inhibitors of hHexB than of hOGA. Sulfonylhydrazone **5f** is the strongest inhibitor of both enzymes and the most selective towards hHexB after **5b** (**5b** is also the least potent inhibitor for both enzymes). Analogously to the parent structure PUGNAc, the newly prepared derivatives **5a–f** suffer from virtually no selectivity towards any of the tested enzymes, which suggests that the affinity of the aglycone part of the inhibitors might be similar for both glycosidases.

Table 3. Binding affinities of compounds **5** toward hOGA and hHexB enzymes compared to those of some previously known inhibitors.

Compound	K_i (nM)		$K_{i(\text{hHexB})}/K_{i(\text{hOGA})}^a$	
	hOGA	hHexB		
PUGNAc		46 [10]	36 [10]	0.8
2-acetamido-2-deoxy-D-glucono-1,5-lactone 4-(2-naphthyl)-semicarbazone		36 [12]	47 [12]	1.3
5a		78 ± 1	21 ± 2	0.27
5b		230 ± 17	48 ± 4	0.21
5c		95 ± 11	45 ± 3	0.43
5d		70 ± 3	39 ± 2	0.56
5e		30 ± 2	30 ± 3	1
5f		27 ± 7	6.8 ± 1.8	0.25

^a The ratio defines selectivity towards hOGA.

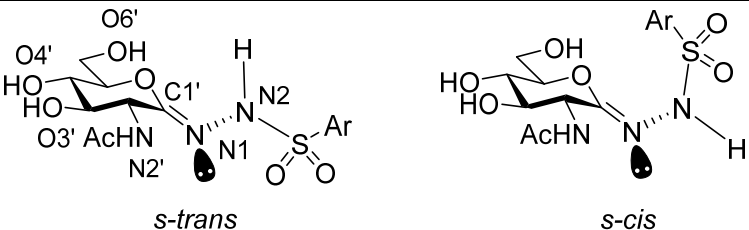
2.3. Computationally Predicted Enzyme–Inhibitor Binding in hOGA

To predict and analyze the hOGA binding modes of inhibitors **5**, Prime protein–ligand refinements [21] were performed based on their successful application to the previously reported 2-acetamido-2-deoxy-D-glucono-1,5-lactone semicarbazone series of inhibitors [12]. In this previous study, it was found that Glide native ligand redocking calculations (PDB code: 5UHO) did not reproduce the PUGNAc crystallographic conformation, specifically the orientation of the phenylurethane moiety, so that the Prime refinement and a QM/MM approach was applied [12]. In the present case, however, due to the shortened length of the linker and the greater variance in the structures of the target 2-acetamido-2-deoxy-D-glucono-1,5-lactone arenesulfonylhydrazones compared to PUGNAc in the

starting model hOGA–PUGNAc complex (PDB code: 5UHO), refinements were performed in the hierarchical optimization mode (as opposed to the local optimization mode), which involved systematic sampling of inhibitor positions, orientations and conformations, along with enzyme binding site residues. The five output models for each inhibitor were then further refined in the local optimization mode (releasing hydrogen bond constraints, cf. Experimental details), but also used in QM/MM optimizations that should, in theory, better describe the energetic features of the predicted binding modes. More specifically, QM/MM has important applications in areas where standard force field-based methods may not be entirely accurate. A QM description of this novel set of compounds would address any potential shortcomings in force field parameters, particularly in the description of key dihedrals such as the rotations around the N1–N2 bond (cf. atom numbering scheme in Table 4) and the surrounding dihedrals. The binding of **5a–f** to hOGA was predicted using this approach; the PUGNAc inhibitor was also included for initial validation by geometrically comparing its predicted complex with its solved crystallographic structure (PDB code: 5UHO).

The energy results from the Prime enzyme–inhibitor refinements and QM/MM calculations are shown in Table 4. In some cases, close to equivalent poses were obtained and coincided with similar absolute/relative energies. As expected, all the energies are lower following the second Prime enzyme–inhibitor refinement in the local optimization mode; the lowest energy enzyme–inhibitor complex pose was also subject to change in some cases. As mentioned, QM/MM approaches can provide a more accurate picture of the preferred binding mode [22,23]. For PUGNAc, the lowest energy QM/MM optimized poses 4 and 5 were equivalent based on energy and RMSD (heavy atoms) comparisons. Comparing these predicted enzyme–inhibitor models with the crystal structure complex following backbone superimposition, the RMSDs (heavy atoms) for ligand and flexible binding site residues were just 0.762 Å and 0.452 Å, respectively, an initial validation of the refinement protocol. For **5a–f**, with the inhibitors described by QM, the key conformations through rotations around the N1–N2 bond (and associated dihedrals) can be more accurately described. Therefore, it was not overly surprising that there was a more considerable change in preferred binding mode following the QM/MM optimizations compared to the Prime enzyme–inhibitor refinements, both in terms of geometry and associated energetics. Most importantly, all inhibitors were observed to have a preference for the *s-cis* binding conformation around the N1–N2 bond (cf. Table 4), conformations that were originally ranked lower in the initial Prime refinements (where the preference was generally *s-trans*). The QM/MM optimized lowest energy complexes had inhibitor C1′=N1–N2–H dihedral angles in a similar range -168.0° to -172.2° for **5a–e**, and slightly less planar (-154.4°) for **5f**. It is noted that solvation effects are not accounted for in the QM/MM optimizations.

Table 4. Energy results for the predicted binding poses of PUGNAc and the six inhibitors **5a-f** with hOGA. The atom numbering scheme and the two key potential binding conformations (*s-trans* and *s-cis*) around the N1–N2 bond are highlighted.

Inhibitor/pose	Prime Hierarchical		Prime Local		QM/MM		Dihedral ^a (°) C1'=N1-N2-H
	Prime Energy (kcal/mol)	Relative Energy (kcal/mol)	Prime Energy (kcal/mol)	Relative Energy (kcal/mol)	Absolute Energy (Hartrees)	Relative Energy (kcal/mol)	
							
PUGNAc							
Pose 1	-34,316.1	0.0	-34,320.1	0.6	-1328.97031	1.2	-
Pose 2	-34,315.9	0.2	-34,320.7	0.0	-1328.96987	1.5	-
Pose 3	-34,315.8	0.3	-34,320.1	0.6	-1328.97033	1.2	-
Pose 4	-34,315.6	0.5	-34,319.9	0.8	-1328.97226	0.0	-
Pose 5	-34,315.6	0.5	-34,320.5	0.2	-1328.97227	0.0	-
5a							
Pose 1	-34,317.1	0.0	-34,320.7	0.9	-1728.25188	8.8	-14.9
Pose 2	-34,315.8	1.3	-34,318.0	3.6	-1728.26592	0.0	-172.2
Pose 3	-34,315.2	1.9	-34,320.2	1.4	-1728.25192	8.8	-15.1
Pose 4	-34,315.1	2.0	-34,318.6	3.0	-1728.26597	0.0	-171.8
Pose 5	-34,314.8	2.3	-34,321.6	0.0	-1728.25203	8.7	-15.1
5b							
Pose 1	-34,303.5	0.0	-34,310.8	0.0	-2025.91547	13.3	8.1
Pose 2	-34,302.4	1.1	-34,304.6	6.2	-2025.93662	0.0	-168.0
Pose 3	-34,302.0	1.5	-34,305.1	5.7	-2025.92286	8.6	-22.0
Pose 4	-34,301.5	2.0	-34,305.0	5.8	-2025.92249	8.9	-21.4
Pose 5	-34,301.5	2.0	-34,305.2	5.6	-2025.92290	8.6	-22.0
5c							
Pose 1	-34,318.0	0.0	-34,322.8	0.3	-1788.16899	8.7	-17.9
Pose 2	-34,317.5	0.5	-34,323.1	0.0	-1788.16894	8.8	-17.5
Pose 3	-34,317.4	0.6	-34,322.3	0.8	-1788.18292	0.0	-170.7
Pose 4	-34,317.3	0.7	-34,321.8	1.3	-1788.18290	0.0	-170.6
Pose 5	-34,316.8	1.2	-34,319.1	4.0	-1788.18236	0.4	-149.3
5d							
Pose 1	-34,318.3	0.0	-34,320.1	0.2	-2148.53075	9.0	-19.6
Pose 2	-34,316.6	1.7	-34,320.3	0.0	-2148.53084	8.9	-19.7
Pose 3	-34,315.9	2.4	-34,319.4	0.9	-2148.53121	8.7	-20.5
Pose 4	-34,315.8	2.5	-34,319.1	1.2	-2148.53073	9.0	-19.3
Pose 5	-34,315.1	3.2	-34,319.5	0.8	-2148.54505	0.0	-169.2
5e							
Pose 1	-34,303.0	0.0	-34,308.7	0.0	-1842.54825	8.6	-11.8
Pose 2	-34,302.9	0.1	-34,306.0	2.7	-1842.56165	0.2	-169.3
Pose 3	-34,300.8	2.2	-34,306.6	2.1	-1842.56197	0.0	-169.6
Pose 4	-34,300.6	2.4	-34,306.9	1.8	-1842.56199	0.0	-169.5
Pose 5	-34,300.3	2.7	-34,306.7	2.0	-1842.56189	0.1	-169.7
5f							

Pose 1	-34,308.4	0.0	-34,311.4	1.5	-1842.54544	4.7	-0.8
Pose 2	-34,304.6	3.8	-34,309.9	3.0	-1842.54384	5.7	3.6
Pose 3	-34,303.2	5.2	-34,312.9	0.0	-1842.53822	9.2	-2.1
Pose 4	-34,302.0	6.4	-34,305.5	7.4	-1842.54411	5.6	-169.9
Pose 5	-34,301.4	7.0	-34,308.7	4.2	-1842.55296	0.0	-154.1

^a Dihedral angles close to 0° correspond to *s-trans* and those close to ±180° to *s-cis* conformations.

The predicted QM/MM optimized binding geometries of the phenyl-substituted inhibitors **5a–d** with hOGA are similar and shown in Figure 2. There are key interactions similar to those reported previously for the 2-acetamido-2-deoxy-D-glucono-1,5-lactone semicarbazone series of compounds and PUGNAc [12]. Notably, the *N*-acetyl-glucosamine moiety hydrogen bond interactions are conserved as follows (cf. atom numbering in Table 4): inhibitor O3'-hydroxyl with both Gly67 backbone O and Lys98 sidechain; O4'-hydroxyl O with Asn313 sidechain amide and Asp285 sidechain carboxylate; O6' hydroxyl with Asp285 sidechain carboxylate; and the *N*-acetyl group has hydrogen bonds involving N2'H with the Asp174 sidechain carboxylate and acetyl carbonyl O with the Asn280 sidechain amide. In terms of the sulfonylhydrazone linker between the *N*-acetyl-glucosamine and phenyl groups, N2H hydrogen bonds with the Tyr219 sidechain hydroxyl O atom and there is also potential for hydrogen bonding of this hydroxyl with ligand N1 atoms. The differences in **5a–d** are their phenyl *para*-substituents. All ligand phenyls have favorable interactions with the Val254 sidechain. There are interactions between the *para*-substituents (-CH₃, -CF₃, -F, and -Cl) and hydrophobic sidechains of Tyr286 and Val255. The CF₃ group (**5b**) is shifted away from Tyr286, an interaction which may be related to its lower hOGA inhibition potency ($K_i = 230$ nM); alternatively, the methyl-substituted **5a** ($K_i = 78$ nM) can form good CH- π contacts with the Tyr286 ring. There are also NH-halogen (enzyme-inhibitor, respectively) interactions for **5b–d** involving the Val255 backbone NH. Notably, in the case of the most potent phenyl-substituted compound **5d** (Cl substituent, $K_i = 70$ nM), the halogen-hydrogen bond donor (HBD) interactions are consistent with a survey of crystal structure data; the predicted C-Cl-HBD angle (85.4°) and the HBD-Cl (4.4 Å) distance are close to the observed most prominent values (HBD defined by the NH nitrogen atom) [24].

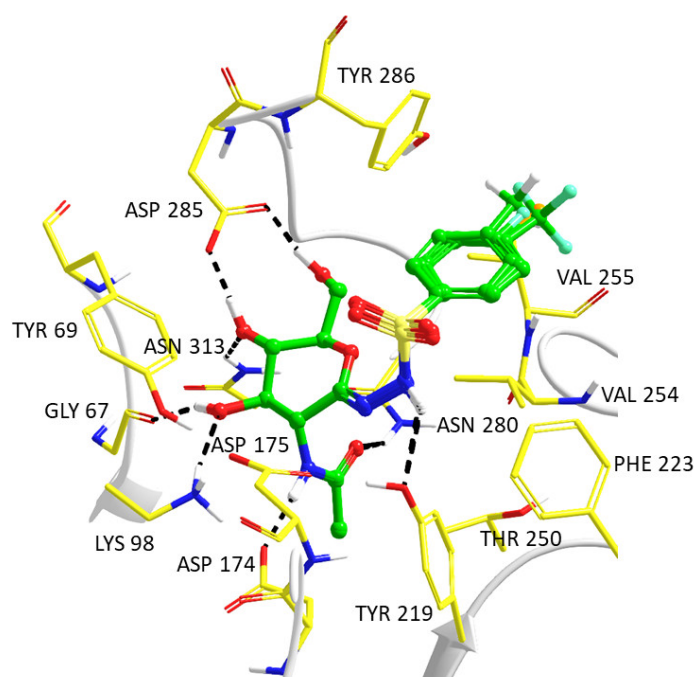


Figure 2. Predicted model complexes of the phenyl-substituted analogs **5a–d** following QM/MM optimizations of complexes from Prime hierarchical optimization mode protein–ligand refinements.

Shown are the relative positions of the inhibitors following enzyme backbone superimposition; the protein from the predicted hOGA-5a complex only is displayed for clarity. Fluorine ligand atoms are shown as cyan and chlorine as orange.

The most potent hOGA inhibitors were the naphthyl analogs, **5e** (2-naphthyl) and **5f** (1-naphthyl), with these ligands close to equipotent (K_i -s \sim 30 nM). The predicted binding of these inhibitors from the QM/MM optimizations are shown in Figure 3A,B, respectively. Both ligands are able to exploit favorable interactions with the Val254 sidechain and have the potential for NH- π contacts from the backbone NH of the flexible loop residue Val255, all of which could be the source of their observed superior potencies. The 2-naphthyl substituent of **5e** is also aligned with the Tyr286 ring in a T-shaped configuration for π - π stacking interactions with a ring centroid-centroid distance of 5.1 Å. This can be considered consistent with geometric preferences of protein-ligand T-shaped π - π interactions from Protein Data Bank analysis, with T-shaped binding conformations also found to be the most predominant [25]. In the case of **5f**, a 180° flip of the 1-naphthalene ring around the S-C(Ar) bond would lead to alternate π - π interactions with Phe223.

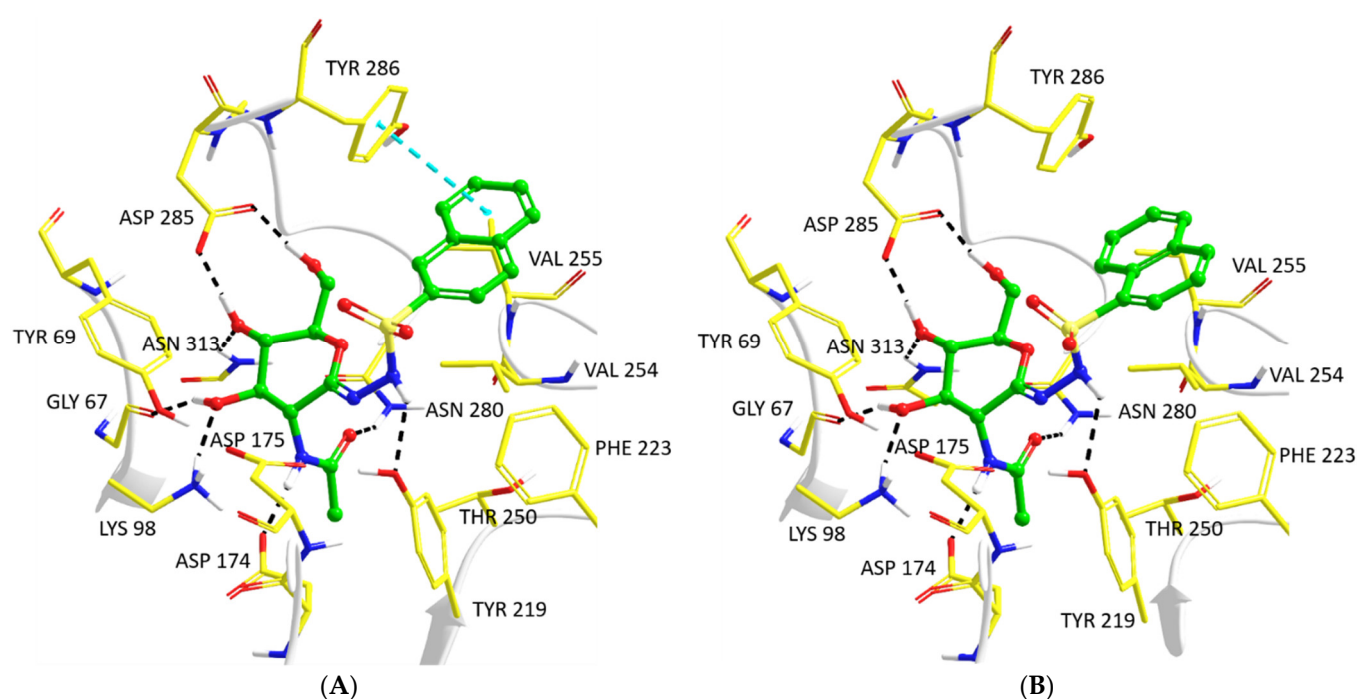


Figure 3. Predicted models of hOGA-5e (A) and hOGA-5f (B) following QM/MM optimizations of complexes from Prime hierarchical optimization mode enzyme-inhibitor refinements.

3. Materials and Methods

3.1. Synthesis

3.1.1. General Methods

Melting points were measured on a Kofler hot stage and are uncorrected. Optical rotations were determined using a Jasco P-2000 (Easton, MD, USA) polarimeter at room temperature. 1D NMR spectra were recorded using Bruker AM Avance 360 (360/90 MHz for $^1\text{H}/^{13}\text{C}$) or Bruker 400 (400/100 MHz for $^1\text{H}/^{13}\text{C}$) spectrometers (Bruker, Karlsruhe, Germany). Chemical shifts are referenced to TMS as an internal reference (^1H) or to residual solvent signals (^{13}C). 2D ^1H - ^{13}C HSQC-CLIP-COSY experiment with HSQC vs. COSY peak sign editing [26] and 2D ^1H - ^1H EASY ROESY experiment [19] with 300 ms mixing time were carried out for the unambiguous structure elucidation of compound **5d** on a Bruker Avance Neo 700 MHz NMR spectrometer (Bruker, Karlsruhe, Germany) equipped with a Prodigy TCI cryoprobe. Mass spectra were recorded with MicroTOF-Q type Qq-TOF MS

and maXis II UHR ESI-QTOF MS (Bruker Daltonik, Bremen, Germany) instruments in the positive ion mode with the electrospray ionization or atmospheric pressure chemical ionization technique. TLC plates were visualized under UV light and by spray reagent with gentle heating (the plate was sprayed with the following solution: abs. EtOH (95 mL), conc. H₂SO₄ (5 mL), and anisaldehyde (1 mL)). Kieselgel 60 (Merck, particle size 0.063–0.200 mm) was used for column chromatography. CH₂Cl₂ was distilled from P₂O₅ and stored over 4 Å molecular sieves. *p*-Toluenesulfonyl hydrazide (**2a**) was purchased from Sigma-Aldrich Ltd. (Budapest, Hungary). 2-Acetamido-3,4,6-tri-*O*-acetyl-2-deoxy- α,β -D-glucopyranose (**1**) [16,17], substituted benzenesulfonyl hydrazides (**2b–d**), and 2- or 1-naphthalenesulfonyl hydrazides (**2e–f**) [18] were synthesized according to literature procedures. Unless otherwise indicated, all chemicals used in the biochemical experiments were of analytical grade and were purchased from Sigma-Aldrich Ltd. (Budapest, Hungary).

3.1.2. General Procedure A for the Synthesis of 1-(2-Acetamido-3,4,6-tri-*O*-acetyl-2-deoxy- β -D-glucopyranosyl)-2-arenesulfonyl Hydrazines (**3**)

A solution of 200 mg (0.58 mmol) of 2-acetamido-3,4,6-tri-*O*-acetyl-2-deoxy- α,β -D-glucopyranose (**1**), 0.87 mmol of an arenesulfonyl hydrazide **2** and 0.058 mmol of *p*-toluenesulfonic acid in 4 mL of chloroform was boiled under reflux for 4 h until the reaction was complete (monitored by TLC hexane:acetone, 1:1). The mixture was cooled in an ice bath and the white precipitate was filtered off. If the reagents contaminated the product, column chromatography was performed (hexane:acetone, 3:2).

1-(2-Acetamido-3,4,6-tri-*O*-acetyl-2-deoxy- β -D-glucopyranosyl)-2-(*p*-toluenesulfonyl) Hydrazine (**3a**)

Prepared according to General procedure A from 200 mg (0.58 mmol) of **1**, 160 mg (0.87 mmol) of *p*-toluenesulfonyl hydrazide (**2a**) and 12 mg (0.058 mmol) *p*-toluenesulfonic acid. The excess of the reagent was filtered off from the reaction mixture and the solvent was evaporated: 230 mg (77%) of white powder was isolated. m.p.: 172–174 °C; $[\alpha]_D^{25} = -60$ ($c = 0.43$, CHCl₃). ¹H NMR (CDCl₃) δ (ppm): 7.72 (d, 2H, $J = 7.7$ Hz, Ar), 7.31 (d, 2H, $J = 7.6$ Hz, Ar), 6.65 (s, 1H, NH), 6.13 (d, 1H, $J = 8.5$ Hz, NH), 5.28 (pt, 1H, $J = 9.8$ Hz, H-3), 4.98 (pt, 1H, $J = 9.6$ Hz, H-4), 4.41 (pt, 1H, $J = 8.4$ Hz, H-1), 4.28 (d, 1H, $J = 7.9$ Hz, NH), 4.19 (dd, 1H, $J = 3.8$, 12.1 Hz, H-6a), 4.09 (dd, 1H, $J = 1.8$, 12.1 Hz, H-6b), 3.86 (ddd ('q'), 1H, $J = 9.4$ Hz, H-2), 3.70–3.66 (m, 1H, H-5), 2.43 (s, 3H, CH₃), 2.08, 2.03, 2.02, 1.99 (4 s, 12H, 4 CH₃). ¹³C NMR (CDCl₃) δ (ppm): 171.19, 171.09, 170.84, 169.54 (C=O), 144.42, 134.77, 129.68, 128.15 (Ar), 90.10 (C-1), 73.10, 72.59, 68.63 (C-3, C-4, C-5), 62.16 (C-6), 51.97 (C-2), 23.30, 21.68, 20.83, 20.77, 20.69 (5 CH₃). ESI-MS positive mode (m/z): calcd. for C₂₁H₂₉N₃O₁₀S (515.16) $[M + H]^+ = 516.16$, found: $[M + H]^+ = 516.92$.

1-(2-Acetamido-3,4,6-tri-*O*-acetyl-2-deoxy- β -D-glucopyranosyl)-2-(*p*-trifluoromethylbenzenesulfonyl) Hydrazine (**3b**)

Prepared according to General procedure A from 200 mg (0.58 mmol) of **1**, 209 mg (0.87 mmol) of *p*-trifluoromethylbenzenesulfonyl hydrazide (**2b**) and 12 mg (0.058 mmol) *p*-toluenesulfonic acid. The excess of the reagent was filtered off from the reaction mixture, the solvent was removed and the residue was purified by column chromatography: 281 mg (85%) of white powder was isolated. m.p.: 185–187 °C (decomposition); $[\alpha]_D^{25} = -41$ ($c = 0.32$, CH₂Cl₂). ¹H NMR (CDCl₃) δ (ppm): 7.98 (d, 2H, $J = 7.7$ Hz, Ar), 7.79 (t, 2H, $J = 7.7$ Hz, Ar), 6.85 (s, 1H, NH), 6.08 (d, 1H, $J = 8.3$ Hz, NH), 5.23 (pt, 1H, $J = 9.7$ Hz, H-3), 5.00 (pt, 1H, $J = 9.4$ Hz, H-4), 4.46–4.28 (m, 2H, H-1, NH), 4.19 (dd, 1H, $J = 2.9$, 11.7 Hz, H-6a), 4.11 (dd, 1H, $J = 1.3$, 12.2 Hz, H-6b), 3.87 (ddd ('q'), 1H, $J = 8.8$ Hz, H-2), 3.77–3.62 (m, 1H, H-5), 2.08, 2.04, 2.03, 1.98 (4 s, 12H, 4 CH₃). ¹³C NMR (CDCl₃) δ (ppm): 171.32, 171.16, 170.85, 169.51 (C=O), 141.58, 134.94 (q, ² $J_{CF} = 33.6$ Hz), 128.63, 126.26 (q, ⁴ $J_{CF} = 3.6$ Hz, Ar) 126.07 (q, ¹ $J_{CF} = 280.6$ Hz, CF₃), 90.47 (C-1), 73.37, 72.52, 68.45 (C-3, C-4, C-5), 62.10 (C-6), 52.13 (C-2),

23.33, 20.87, 20.79, 20.71 (4 CH₃). ESI-MS positive mode (*m/z*): calcd. for C₂₁H₂₆F₃N₃O₁₀S (569.13) [M + H]⁺ = 570.14, found: [M + H]⁺ = 570.17.

1-(2-Acetamido-3,4,6-tri-*O*-acetyl-2-deoxy-β-D-glucopyranosyl)-2-(*p*-fluorobenzenesulfonyl) Hydrazine (**3c**)

Prepared according to General procedure A from 200 mg (0.58 mmol) of **1**, 165 mg (0.87 mmol) of *p*-fluorobenzenesulfonyl hydrazide (**2c**), and 12 mg (0.058 mmol) *p*-toluenesulfonic acid. The excess of the reagent was filtered off from the reaction mixture, the solvent was removed, and the residue was purified by column chromatography: 259 mg (86%) of white powder was isolated. m.p.: 187–190 °C; [α]_D = −38 (c = 0.30, CH₂Cl₂). ¹H NMR (CDCl₃) δ (ppm): 7.86 (dd, 2H, *J* = 5.0, 8.7 Hz, Ar), 7.20 (t, 2H, *J* = 8.5 Hz, Ar), 6.63 (s, 1H, NH), 6.04 (d, 1H, *J* = 8.5 Hz, NH), 5.24 (pt, 1H, *J* = 9.9 Hz, H-3), 5.00 (pt, 1H, *J* = 9.7 Hz, H-4), 4.40 (pt, 1H, *J* = 9.1 Hz, H-1), 4.30 (d, 1H, *J* = 9.0 Hz, NH), 4.20 (dd, 1H, *J* = 4.5, 12.3 Hz, H-6a), 4.09 (dd, 1H, *J* = 1.2, 12.0 Hz, H-6b), 3.86 (ddd ('q'), 1H, *J* = 9.5 Hz, H-2), 3.68 (ddd, 1H, *J* = 2.2, 4.2, 9.9 Hz, H-5), 2.08, 2.04, 2.03, 1.98 (4 s, 12H, 4 CH₃). ¹³C NMR (CDCl₃) δ (ppm): 171.28, 171.08, 170.83, 169.52 (C=O), 165.66 (d, ¹*J*_{CF} = 255.8 Hz), 133.86, 130.92 (d, ³*J*_{CF} = 9.3 Hz), 116.41 (d, ²*J*_{CF} = 22.7 Hz, Ar), 90.34 (C-1), 73.29, 72.52, 68.44 (C-3, C-4, C-5), 62.11 (C-6), 52.10 (C-2), 23.36, 20.88, 20.81, 20.73 (4 CH₃). ESI-MS positive mode (*m/z*): calcd. for C₂₀H₂₆FN₃O₁₀S (519.13) [M + H]⁺ = 520.14, found: [M + H]⁺ = 520.17.

1-(2-Acetamido-3,4,6-tri-*O*-acetyl-2-deoxy-β-D-glucopyranosyl)-2-(*p*-chlorobenzenesulfonyl) Hydrazine (**3d**)

Prepared according to General procedure A from 200 mg (0.58 mmol) of **1**, 180 mg (0.87 mmol) of *p*-chlorobenzenesulfonyl hydrazide (**2d**), and 12 mg (0.058 mmol) *p*-toluenesulfonic acid. The excess of the reagent was filtered off from the reaction mixture, the solvent was removed, and the residue was purified by column chromatography: 277 mg (89%) of white powder was isolated. m.p.: 195–198 °C (decomposition); [α]_D = −42 (c = 0.23, CH₂Cl₂). ¹H NMR (CDCl₃) δ (ppm): 7.77 (d, 2H, *J* = 8.6 Hz, Ar), 7.49 (d, 2H, *J* = 8.6 Hz, Ar), 6.46 (s, 1H, NH), 5.85 (d, 1H, *J* = 8.5 Hz, NH), 5.22 (pt, 1H, *J* = 10.0 Hz, H-3), 5.01 (pt, 1H, *J* = 9.7 Hz, H-4), 4.39 (pt, 1H, *J* = 9.1 Hz, H-1), 4.26 (d, 1H, *J* = 8.9 Hz, NH), 4.20 (dd, 1H, *J* = 4.6, 12.4 Hz, H-6a), 4.10 (dd, 1H, *J* = 1.9, 12.3 Hz, H-6b), 3.86 (ddd ('q'), 1H, *J* = 9.6 Hz, H-2), 3.66 (ddd, 1H, *J* = 2.4, 4.6, 10.2 Hz, H-5), 2.09, 2.04, 2.03, 1.98 (4 s, 12H, 4 CH₃). ¹³C NMR (CDCl₃) δ (ppm): 171.34, 171.00, 170.78, 169.49 (C=O), 140.22, 136.38, 129.55, 129.47 (Ar), 90.41 (C-1), 73.43, 72.52, 68.35 (C-3, C-4, C-5), 62.08 (C-6), 52.18 (C-2), 23.40, 20.90, 20.81, 20.74 (4 CH₃). ESI-MS positive mode (*m/z*): calcd. for C₂₀H₂₆ClN₃O₁₀S (535.10) [M + H]⁺ = 536.11, found: [M + H]⁺ = 536.17.

1-(2-Acetamido-3,4,6-tri-*O*-acetyl-2-deoxy-β-D-glucopyranosyl)-2-(2-naphthalenesulfonyl) Hydrazine (**3e**)

Prepared according to General procedure A from 200 mg (0.58 mmol) of **1**, 193 mg (0.87 mmol) of 2-naphthalenesulfonyl hydrazide (**2e**), and 12 mg (0.058 mmol) *p*-toluenesulfonic acid. The excess of the reagent was filtered off from the reaction mixture, the solvent was removed, and the residue was purified by column chromatography: 243 mg (76%) of white powder was isolated. m.p.: 145–148 °C; [α]_D = −33 (c = 0.23, CH₂Cl₂). ¹H NMR (CDCl₃) δ (ppm): 8.41 (s, 1H, Ar), 7.97–7.86 (m, 3H, Ar), 7.80 (dd, 1H, *J* = 1.8, 8.7 Hz, Ar), 7.65 (td, 1H, *J* = 1.6, 6.8 Hz, Ar), 7.60 (td, 1H, *J* = 1.2, 6.5 Hz, Ar), 6.99 (s, 1H, NH), 6.30 (d, 1H, *J* = 8.9 Hz, NH), 5.26 (pt, 1H, *J* = 10.1 Hz, H-3), 4.96 (pt, 1H, *J* = 9.8 Hz, H-4), 4.45–4.37 (m, 2H, H-1, NH), 4.15 (dd, 1H, *J* = 4.5, 12.4 Hz, H-6a), 4.06 (dd, 1H, *J* = 2.2, 12.3 Hz, H-6b), 3.86 (ddd ('q'), 1H, *J* = 9.3 Hz, H-2), 3.66 (ddd, 1H, *J* = 2.3, 4.3, 10.0 Hz, H-5), 2.04, 2.02, 2.00, 1.95 (4 s, 12H, 4 CH₃). ¹³C NMR (CDCl₃) δ (ppm): 171.22, 171.07, 170.87, 169.54 (C=O), 135.17, 134.66, 132.09, 129.84, 129.33, 129.30, 129.20, 128.06, 127.73, 122.95 (Ar), 90.17 (C-1), 73.05, 72.62, 68.62 (C-3, C-4, C-5), 62.11 (C-6), 51.94 (C-2), 23.25, 20.80, 20.75, 20.67 (4

CH₃). ESI-MS positive mode (*m/z*): calcd. for C₂₄H₂₉N₃O₁₀S (551.16) [M + H]⁺ = 552.16, found: [M + H]⁺ = 552.08.

1-(2-Acetamido-3,4,6-tri-*O*-acetyl-2-deoxy-β-D-glucopyranosyl)-2-(1-naphthalenesulfonyl) Hydrazine (**3f**)

Prepared according to General procedure A from 200 mg (0.58 mmol) of **1**, 193 mg (0.87 mmol) of 1-naphthalenesulfonyl hydrazide (**2f**), and 12 mg (0.058 mmol) *p*-toluenesulfonic acid. The excess of the reagent was filtered off from the reaction mixture, the solvent was removed, and the residue was purified by column chromatography: 285 mg (89%) of colorless foam was isolated. [α]_D = −19 (c = 0.22, CH₂Cl₂). ¹H NMR (CDCl₃) δ (ppm): 8.64 (d, 1H, *J* = 8.6 Hz, Ar), 8.24 (dd, 1H, *J* = 1.1, 7.4 Hz, Ar), 8.11 (d, 1H, *J* = 8.2 Hz, Ar), 7.95 (d, 1H, *J* = 7.6 Hz, Ar), 7.67 (td, 1H, *J* = 1.4, 7.1 Hz, Ar), 7.61 (td, 1H, *J* = 1.2, 8.1 Hz, Ar), 7.53 (t, 1H, *J* = 7.6 Hz, Ar), 6.96 (s, 1H, NH), 5.99 (d, 1H, *J* = 8.9 Hz, NH), 5.14 (pt, 1H, *J* = 10.0 Hz, H-3), 4.87 (pt, 1H, *J* = 9.7 Hz, H-4), 4.33 (d, 1H, *J* = 8.0 Hz, NH), 4.26 (t, 1H, *J* = 9.0 Hz, H-1), 4.05 (dd, 1H, *J* = 4.5, 12.4 Hz, H-6a), 4.00 (dd, 1H, *J* = 2.5, 12.4 Hz, H-6b), 3.79 (ddd ('q'), 1H, *J* = 9.2 Hz, H-2), 3.54 (ddd, 1H, *J* = 2.6, 4.3, 10.1 Hz, H-5), 2.06, 2.00, 1.99, 1.90 (4 s, 12H, 4 CH₃). ¹³C NMR (CDCl₃) δ (ppm): 171.15, 171.05, 170.80, 169.47 (C=O), 135.23, 134.27, 132.55, 131.58, 129.24, 128.59, 128.43, 127.11, 124.65, 124.02 (Ar), 89.94 (C-1), 73.06, 72.58, 68.49 (C-3, C-4, C-5), 62.12 (C-6), 51.83 (C-2), 23.23, 20.85, 20.75, 20.67 (4 CH₃). ESI-MS positive mode (*m/z*): calcd. for C₂₄H₂₉N₃O₁₀S (551.16) [M + H]⁺ = 552.16, found: [M + H]⁺ = 552.08.

3.1.3. General Procedure B for the Synthesis of 2-Acetamido-3,4,6-tri-*O*-acetyl-2-deoxy-D-glucono-1,5-lactone Arenesulfonylhydrazones (**4**)

Activated MnO₂ (quantity specified with the particular compounds) was added to a solution of 100 mg of compound **3** in anhydrous CH₂Cl₂. The mixture was boiled for 20 h. After the reaction was completed (TLC hexane:acetone, 1:1), the MnO₂ was filtered off under diminished pressure, and the filtrate was concentrated. The residue was purified by column chromatography (hexane:acetone, 2:1).

2-Acetamido-3,4,6-tri-*O*-acetyl-2-deoxy-D-glucono-1,5-lactone *p*-Toluenesulfonylhydrazone (**4a**)

Compound **4a** was obtained according to General procedure B from **3a** (100 mg, 0.194 mmol) in 4 mL of anhydrous CH₂Cl₂, and 340 mg (3.88 mmol) of activated MnO₂. The crude product was purified by column chromatography to give 69 mg (69%) of white powder. m.p.: 137–141 °C; [α]_D = +15 (c = 0.48, CHCl₃). ¹H NMR (CDCl₃) δ (ppm): 8.07 (s, 1H, NH), 7.75 (d, 2H, *J* = 8.3 Hz, Ar), 7.31 (d, 2H, *J* = 8.3 Hz, Ar), 6.15 (d, 1H, *J* = 8.7 Hz, NH), 5.29 (pt, 1H, *J* = 9.2 Hz, H-3), 5.19 (pt, 1H, *J* = 9.2 Hz, H-4), 4.76 (dd, 1H, *J* = 8.7, 9.2 Hz, H-2), 4.30–4.21 (m, 3H, H-6a, H-6b, H-5), 2.43 (s, 3H, CH₃), 2.08, 2.04, 2.04, 2.00 (4 s, 12H, 4 CH₃). ¹³C NMR (CDCl₃) δ (ppm): 170.51, 170.47, 170.42, 169.19 (C=O), 146.12 (C=N), 144.55, 134.97, 129.74, 127.99 (Ar), 77.05, 71.81, 67.19 (C-3, C-4, C-5), 61.29 (C-6), 50.20 (C-2), 23.09, 21.74, 20.73, 20.60 (5 CH₃). ESI-MS positive mode (*m/z*): calcd. for C₂₁H₂₇N₃O₁₀S (513.14) [M + H]⁺ = 514.15, found: [M + H]⁺ = 514.25.

2-Acetamido-3,4,6-tri-*O*-acetyl-2-deoxy-D-glucono-1,5-lactone *p*-Trifluoromethylbenzenesulfonylhydrazone (**4b**)

Compound **4b** was obtained according to General procedure B from **3b** (100 mg, 0.176 mmol) in 4 mL anhydrous CH₂Cl₂ and 306 mg (3.52 mmol) of activated MnO₂. The crude product was purified by column chromatography to give 60 mg (60%) of white powder. m.p.: 182–185 °C (decomposition); [α]_D = +16 (c = 0.25, CH₂Cl₂). ¹H NMR (CDCl₃) δ (ppm): 8.21 (s, 1H, NH), 8.01 (d, 2H, *J* = 8.2 Hz, Ar), 7.79 (d, 2H, *J* = 8.4 Hz, Ar), 6.12 (d, 1H, *J* = 8.6 Hz, NH), 5.29 (pt, 1H, *J* = 9.5 Hz, H-3), 5.22 (pt, 1H, *J* = 9.6 Hz, H-4), 4.73 (dd, 1H, *J* = 8.7, 9.7 Hz, H-2), 4.38–4.25 (m, 3H, H-6a, H-6b, H-5), 2.07, 2.05, 2.05, 1.99 (4 s, 12H, 4 CH₃). ¹³C NMR (CDCl₃) δ (ppm): 170.60, 170.56, 170.43, 169.20 (C=O), 146.95 (C=N),

141.63, 135.06 (q, $^2J_{CF} = 33.3$ Hz), 128.50, 126.24 (q, $^4J_{CF} = 3.4$ Hz, Ar) 123.26 (q, $^1J_{CF} = 271.7$ Hz, CF₃), 77.13, 71.50, 67.25 (C-3, C-4, C-5), 61.31 (C-6), 50.31 (C-2), 22.99, 20.67, 20.55 (4 CH₃). ESI-MS positive mode (m/z): calcd. for C₂₁H₂₄F₃N₃O₁₀S (567.11) [M + H]⁺ = 568.12, found: [M + H]⁺ = 568.14.

2-Acetamido-3,4,6-tri-*O*-acetyl-2-deoxy-D-glucono-1,5-lactone *p*-Fluorobenzenesulfonylhydrazone (**4c**)

Compound **4c** was obtained according to General procedure B from **3c** (100 mg, 0.193 mmol) in 4 mL anhydrous CH₂Cl₂ and 336 mg (3.86 mmol) of activated MnO₂. The crude product was purified by column chromatography to give 72 mg (72%) of amorphous foam. [α]_D = +14 (c = 0.24, CH₂Cl₂). ¹H NMR (CDCl₃) δ (ppm): 8.16 (s, 1H, NH), 7.89 (dd, 2H, $J = 5.0, 8.9$ Hz, Ar), 7.19 (t, 2H, $J = 8.6$ Hz, Ar), 6.20 (d, 1H, $J = 8.6$ Hz, NH), 5.30 (pt, 1H, $J = 9.1$ Hz, H-3), 5.21 (pt, 1H, $J = 9.6$ Hz, H-4), 4.75 (dd, 1H, $J = 8.7, 10.0$ Hz, H-2), 4.38–4.22 (m, 3H, H-6a, H-6b, H-5), 2.08, 2.05, 2.04, 2.00 (4 s, 12H, 4 CH₃). ¹³C NMR (CDCl₃) δ (ppm): 170.55, 170.48, 170.45, 169.19 (C=O), 146.48 (C=N), 165.68 (d, $^1J_{CF} = 256.1$ Hz), 134.01 (d, $^4J_{CF} = 3.1$ Hz), 130.80 (d, $^3J_{CF} = 9.4$ Hz), 116.41 (d, $^2J_{CF} = 22.7$ Hz, Ar), 77.12, 71.61, 67.23 (C-3, C-4, C-5), 61.30 (C-6), 50.26 (C-2), 23.07, 20.73, 20.69, 20.59 (4 CH₃). ESI-MS positive mode (m/z): calcd. for C₂₀H₂₄FN₃O₁₀S (517.12) [M + H]⁺ = 518.12, found: [M + H]⁺ = 518.17.

2-Acetamido-3,4,6-tri-*O*-acetyl-2-deoxy-D-glucono-1,5-lactone *p*-Chlorobenzenesulfonylhydrazone (**4d**)

Compound **4d** was obtained according to General procedure B from **3d** (100 mg, 0.187 mmol) in 4 mL anhydrous CH₂Cl₂ and 325 mg (3.74 mmol) of activated MnO₂. The crude product was purified by column chromatography to give 77 mg (77%) of amorphous foam. [α]_D = +24 (c = 0.25, CH₂Cl₂). ¹H NMR (CDCl₃) δ (ppm): 8.19 (s, 1H, NH), 7.80 (d, 2H, $J = 8.6$ Hz, Ar), 7.49 (d, 2H, $J = 8.6$ Hz, Ar), 6.21 (d, 1H, $J = 8.7$ Hz, NH), 5.30 (pt, 1H, $J = 9.1$ Hz, H-4), 5.22 (pt, 1H, $J = 9.6$ Hz, H-3), 4.74 (dd, 1H, $J = 8.7, 9.6$ Hz, H-2), 4.36–4.20 (m, 3H, H-6a, H-6b, H-5), 2.08, 2.05, 2.04, 2.00 (4 s, 12H, 4 CH₃). ¹³C NMR (CDCl₃) δ (ppm): 170.49, 170.43, 170.37, 169.14 (C=O), 146.58 (C=N), 140.10, 136.39, 129.36, (Ar), 77.02, 71.49, 67.14 (C-3, C-4, C-5), 61.23 (C-6), 50.21 (C-2), 23.01, 20.66, 20.64, 20.53 (4 CH₃). ESI-MS positive mode (m/z): calcd. for C₂₀H₂₄ClN₃O₁₀S (533.09) [M + H]⁺ = 534.09, found: [M + H]⁺ = 534.08.

2-Acetamido-3,4,6-tri-*O*-acetyl-2-deoxy-D-glucono-1,5-lactone 2-Naphthalenesulfonylhydrazone (**4e**)

Compound **4e** was obtained according to General procedure B from **3e** (100 mg, 0.181 mmol) in 4 mL anhydrous CH₂Cl₂ and 315 mg (3.62 mmol) of activated MnO₂. The crude product was purified by column chromatography to give 56 mg (56 %) of amorphous foam. [α]_D = +26 (c = 0.25, CH₂Cl₂). ¹H NMR (CDCl₃) δ (ppm): 8.47 (s, 1H, Ar), 8.06 (s, 1H, NH), 8.00–7.88 (m, 3H, Ar), 7.84 (dd, 1H, $J = 1.8, 8.7$ Hz, Ar), 7.70–7.57 (m, 2H, Ar), 6.01 (d, 1H, $J = 8.7$ Hz, NH), 5.26 (pt, 1H, $J = 9.0$ Hz, H-4), 5.17 (pt, 1H, $J = 9.6$ Hz, H-3), 4.72 (dd, 1H, $J = 8.8, 9.7$ Hz, H-2), 4.33–4.16 (m, 3H, H-6a, H-6b, H-5), 2.04, 2.03, 2.01, 1.94 (4 s, 12H, 4 CH₃). ¹³C NMR (CDCl₃) δ (ppm): 170.50, 170.43, 169.18 (C=O), 146.26 (C=N), 135.35, 134.92, 132.22, 129.65, 129.47, 129.39, 129.31, 128.14, 127.79, 122.88 (Ar), 77.21, 71.78, 67.22 (C-3, C-4, C-5), 61.33 (C-6), 50.28 (C-2), 23.06, 20.70, 20.60 (4 CH₃). ESI-MS positive mode (m/z): calcd. for C₂₄H₂₇N₃O₁₀S (549.14) [M + H]⁺ = 550.15, found: [M + H]⁺ = 550.17.

2-Acetamido-3,4,6-tri-*O*-acetyl-2-deoxy-D-glucono-1,5-lactone 1-Naphthalenesulfonylhydrazone (**4f**)

Compound **4f** was obtained according to General procedure B from **3f** (100 mg, 0.181 mmol) in 4 mL anhydrous CH₂Cl₂ and 315 mg (3.62 mmol) of activated MnO₂. The crude product was purified by column chromatography to give 66 mg (66%) of amorphous foam. [α]_D = -19 (c = 0.22, CH₂Cl₂). ¹H NMR (CDCl₃) δ (ppm): 8.76 (d, 1H, $J = 8.6$ Hz, Ar), 8.49 (s, 1H, NH), 8.29 (dd, 1H, $J = 1.1, 7.4$ Hz, Ar), 8.11 (d, 1H, $J = 8.3$ Hz, Ar), 7.95 (d, 1H, J

= 7.5 Hz, Ar), 7.71–7.51 (m, 3H, Ar), 6.09 (d, 1H, $J = 8.6$ Hz, NH), 5.23 (pt, 1H, $J = 9.1$ Hz, H-4), 5.10 (pt, 1H, $J = 9.9$ Hz, H-3), 4.68 (dd, 1H, $J = 8.7, 10.0$ Hz, H-2), 4.33–4.20 (m, 2H, H-6a, H-6b), 4.16 (ddd, 1H, $J = 2.8, 5.8, 9.2$ Hz, H-5), 2.03, 2.00, 1.98, 1.86 (4 s, 12H, 4 CH₃). ¹³C NMR (CDCl₃) δ (ppm): 170.47, 170.32, 170.29, 169.14 (C=O), 146.16 (C=N), 135.24, 134.29, 133.34, 130.82, 129.21, 128.58, 128.45, 127.06, 124.75, 124.21 (Ar), 76.99, 71.94, 67.16 (C-3, C-4, C-5), 61.25 (C-6), 49.97 (C-2), 22.96, 20.67, 20.64, 20.54 (4 CH₃). ESI-MS positive mode (m/z): calcd. for C₂₄H₂₇N₃O₁₀S (549.14) [M + H]⁺ = 550.15, found: [M + H]⁺ = 550.20.

3.1.4. General Procedure C for the Synthesis of 2-Acetamido-2-deoxy-D-glucono-1,5-lactone Arenesulfonylhydrazones (5)

A solution of 100 mg of a compound **4** in 1 mL of MeOH was stirred at 25 °C and 1 mL of a saturated NH₃/MeOH solution was added. After completion of the reaction (4 h, monitored by TLC, CHCl₃: MeOH, 7: 3), the solvent was removed and the residue was purified by column chromatography (CHCl₃: MeOH, 20: 1).

2-Acetamido-2-deoxy-D-glucono-1,5-lactone *p*-Toluenesulfonylhydrazone (5a)

Prepared from **4a** (100 mg, 0.195 mmol) according to General procedure C. The crude product was purified by column chromatography to give 71 mg (94%) of white powder. m.p.: 165–166 °C; $[\alpha]_D^{25} = +55$ ($c = 0.55$, MeOH); ¹H NMR (MeOH-*d*₄) δ (ppm): 7.73 (d, 2H, $J = 8.3$ Hz, Ar), 7.34 (d, 2H, $J = 8.0$ Hz, Ar), 4.31 (d, 1H, $J = 10.1$ Hz, H-2), 3.98 (dd, 1H, $J = 5.8, 10.4$ Hz, H-5), 3.76–3.64 (m, 2H, H-6a, H-6b), 3.56 (dd, 1H, $J = 9.0, 10.0$ Hz, H-3), 3.45 (t, 1H, $J = 9.2$ Hz, H-4), 2.41 (s, 3H, CH₃), 2.02 (s, 3H, CH₃). ¹³C NMR (MeOH-*d*₄) δ (ppm): 174.08 (C=O), 149.44 (C=N), 145.53, 136.57, 130.58, 128.70 (Ar), 82.84, 74.18, 70.24 (C-3, C-4, C-5), 62.50 (C-6), 53.46 (C-2), 22.83 (CH₃), 21.56 (CH₃). ESI-HRMS positive mode (m/z): calcd. for C₁₅H₂₁N₃O₇S (387.1100) [M + Na]⁺ = 410.0992, found: [M + Na]⁺ = 410.0989.

2-Acetamido-2-deoxy-D-glucono-1,5-lactone *p*-Trifluoromethylbenzenesulfonylhydrazone (5b)

Prepared from **4b** (100 mg, 0.176 mmol) according to General procedure C. The crude product was purified by column chromatography to give 65 mg (83%) of white powder. m.p.: 175–176 °C (decomposition); $[\alpha]_D^{25} = +59$ ($c = 0.35$, MeOH); ¹H NMR (MeOH-*d*₄) δ (ppm): 8.04 (d, 2H, $J = 8.2$ Hz, Ar), 7.87 (d, 2H, $J = 8.3$ Hz, Ar), 4.31 (d, 1H, $J = 10.1$ Hz, H-2), 3.99 (dd, 1H, $J = 1.3, 11.7$ Hz, H-5), 3.81–3.65 (m, 2H, H-6a, H-6b), 3.59 (dd, 1H, $J = 9.1, 10.0$ Hz, H-3), 3.46 (t, 1H, $J = 9.2$ Hz, H-4), 2.02 (s, 3H, CH₃). ¹³C NMR (MeOH-*d*₄) δ (ppm): 173.66 (C=O), 149.60 (C=N), 144.60, 135.12 ($q, {}^2J_{CF} = 32.6$ Hz), 129.52, 127.06 ($q, {}^4J_{CF} = 3.6$ Hz, Ar), 121.92 ($q, {}^1J_{CF} = 271.9$ Hz, CF₃), 83.16, 74.30, 70.54 (C-3, C-4, C-5), 62.88 (C-6), 53.65 (C-2), 22.76 (CH₃). ESI-HRMS positive mode (m/z): calcd. for C₁₅H₁₈F₃N₃O₇S (441.0818) [M + Na]⁺ = 464.0710, found: [M + Na]⁺ = 464.0708.

2-Acetamido-2-deoxy-D-glucono-1,5-lactone *p*-Fluorobenzenesulfonylhydrazone (5c)

Prepared from **4c** (100 mg, 0.193 mmol) according to General procedure C. The crude product was purified by column chromatography to give 64 mg (85%) of white powder. m.p.: 175–177 °C; $[\alpha]_D^{25} = +78$ ($c = 0.44$, MeOH); ¹H NMR (MeOH-*d*₄) δ (ppm): 7.90 (dd, 2H, $J = 5.2, 8.6$ Hz, Ar), 7.28 (t, 2H, $J = 8.7$ Hz, Ar), 4.32 (d, 1H, $J = 10.1$ Hz, H-2), 4.00 (dd, 1H, $J = 7.2, 10.9$ Hz, H-5), 3.79–3.65 (m, 2H, H-6a, H-6b), 3.60 (dd, 1H, $J = 8.3, 10.6$ Hz, H-3), 3.47 (t, 1H, $J = 9.0$ Hz, H-4), 2.03 (s, 3H, CH₃). ¹³C NMR (MeOH-*d*₄) δ (ppm): 173.64 (C=O), 149.34 (C=N), 166.57 (d, ${}^1J_{CF} = 252.6$ Hz), 136.46 (d, ${}^4J_{CF} = 3.1$ Hz), 131.69 (d, ${}^3J_{CF} = 9.5$ Hz), 116.96 (d, ${}^2J_{CF} = 23.0$ Hz, Ar), 83.09, 74.34, 70.55 (C-3, C-4, C-5), 62.85 (C-6), 53.58 (C-2), 22.78 (CH₃). ESI-HRMS positive mode (m/z): calcd. for C₁₄H₁₈FN₃O₇S (391.0849) [M + Na]⁺ = 414.0742, found: [M + Na]⁺ = 414.0738.

2-Acetamido-2-deoxy-D-glucono-1,5-lactone *p*-Chlorobenzenesulfonylhydrazone (**5d**)

Prepared from **4d** (100 mg, 0.188 mmol) according to General procedure C. The crude product was purified by column chromatography to give 60 mg (78%) of white powder. m.p.: 180–182 °C (decomposition); $[\alpha]_D^{25} = +78$ ($c = 0.22$, MeOH); $^1\text{H NMR}$ (MeOH- d_4) δ (ppm): 7.82 (d, 2H, $J = 8.8$ Hz, Ar), 7.56 (d, 2H, $J = 8.8$ Hz, Ar), 4.30 (d, 1H, $J = 10.1$ Hz, H-2), 3.97 (dd, 1H, $J = 8.3, 10.5$ Hz, H-5), 3.78–3.65 (m, 2H, H-6a, H-6b), 3.58 (dd, 1H, $J = 9.0, 10.1$, Hz, H-3), 3.46 (t, 1H, $J = 9.2$ Hz, H-4), 2.02 (s, 3H, CH₃). $^{13}\text{C NMR}$ (MeOH- d_4) δ (ppm): 173.66 (C=O), 149.42 (C=N), 140.17, 139.07, 130.46, 130.17 (Ar), 83.16, 74.36, 70.58, (C-3, C-4, C-5), 62.90 (C-6), 53.63 (C-2), 22.76 (CH₃). ESI-HRMS positive mode (m/z): calcd. for C₁₄H₁₈ClN₃O₇S (407.0554) $[\text{M} + \text{Na}]^+ = 430.0446$, found: $[\text{M} + \text{Na}]^+ = 430.0440$.

2-Acetamido-2-deoxy-D-glucono-1,5-lactone 2-Naphthalenesulfonylhydrazone (**5e**)

Prepared from **4e** (100 mg, 0.182 mmol) according to General procedure C. The crude product was purified by column chromatography to give 58 mg (75%) of white powder. m.p.: 172–173 °C; $[\alpha]_D^{25} = +68$ ($c = 0.21$, MeOH); $^1\text{H NMR}$ (MeOH- d_4) δ (ppm): 8.44 (d, 1H, $J = 1.2$ Hz, Ar), 8.06–7.92 (m, 3H, Ar), 7.85 (dd, 1H, $J = 1.8, 8.7$ Hz, Ar), 7.71–7.58 (m, 2H, Ar), 4.29 (d, 1H, $J = 10.0$ Hz, H-2), 3.98 (dd, 1H, $J = 1.3, 11.6$ Hz, H-5), 3.78–3.65 (m, 2H, H-6a, H-6b), 3.54 (dd, 1H, $J = 9.0, 10.0$, Hz, H-3), 3.43 (t, 1H, $J = 9.2$ Hz, H-4), 1.92 (s, 3H, CH₃). $^{13}\text{C NMR}$ (MeOH- d_4) δ (ppm): 173.59 (C=O), 149.28 (C=N), 137.42, 136.38, 133.51, 130.34, 130.04, 129.95, 129.92, 128.96, 128.53, 124.08 (Ar), 83.12, 74.48, 70.55 (C-3, C-4, C-5), 62.91 (C-6), 53.62 (C-2), 22.73 (CH₃). ESI-HRMS positive mode (m/z): calcd. for C₁₈H₂₁N₃O₇S (423.1100) $[\text{M} + \text{Na}]^+ = 446.0992$, found: $[\text{M} + \text{Na}]^+ = 446.0991$.

2-Acetamido-2-deoxy-D-glucono-1,5-lactone 1-Naphthalenesulfonylhydrazone (**5f**)

Prepared from compound **4f** (100 mg, 0.182 mmol) according to General procedure C. The crude product was purified by column chromatography to give 62 mg (80%) of white powder. m.p.: 145–147 °C; $[\alpha]_D^{25} = +58$ ($c = 0.26$, MeOH); $^1\text{H NMR}$ (MeOH- d_4) δ (ppm): 8.81 (d, 1H, $J = 8.5$ Hz, Ar), 8.25 (d, 1H, $J = 7.4$ Hz, Ar), 8.16 (d, 1H, $J = 8.2$ Hz, Ar), 7.99 (d, 1H, $J = 8.0$ Hz, Ar), 7.72–7.55 (m, 3H, Ar), 4.25 (d, 1H, $J = 9.8$ Hz, H-2), 4.00 (dd, 1H, $J = 5.2, 9.9$ Hz, H-5), 3.75–3.66 (m, 2H, H-6a, H-6b), 3.47 (dd, 1H, $J = 8.9, 9.9$, Hz, H-3), 3.40 (t, 1H, $J = 8.9$ Hz, H-4), 1.90 (s, 3H, CH₃). $^{13}\text{C NMR}$ (MeOH- d_4) δ (ppm): 173.48 (C=O), 148.44 (C=N), 135.76, 135.66, 135.59, 131.46, 129.91, 129.84, 128.96, 127.84, 126.23, 125.23 (Ar), 83.27, 74.70, 70.62 (C-3, C-4, C-5), 63.08 (C-6), 53.46 (C-2), 22.70 (CH₃). ESI-HRMS positive mode (m/z): calcd. for C₁₈H₂₁N₃O₇S (423.1100) $[\text{M} + \text{Na}]^+ = 446.0992$, found: $[\text{M} + \text{Na}]^+ = 446.0992$.

3.2. Biochemical Materials and Methods

3.2.1. Protein Expression and Purification

The detailed protocol for the expression of hOGA and the subsequent purification procedure of the recombinant protein have been described in our previous work [12]. The gene construct encoding the full-length human OGA fused to N-terminal His₆-tag was kindly provided by Prof. D. Vocadlo (SFU, Burnaby, BC, Canada). Human β -*N*-acetylhexosaminidase B (hHexB) was expressed in *Pichia pastoris*, and the extracellularly produced enzyme was isolated according to the procedure described by Krejzová et al. [20].

3.2.2. Inhibition Studies

The inhibitory potency of compounds **5a–f** was evaluated against recombinant enzymes hOGA and hHexB. In the case of hOGA inhibition, 4-MU-GlcNAc was used as a substrate at three concentrations (7 μM , 12 μM , and 25 μM) in the reaction mixtures containing 50 mM potassium phosphate buffer (pH 7.5), an inhibitor **5a–f** in a final concentration of 0 to 750 nM, and 3 nM hOGA. In all cases, the enzyme and the inhibitors were preincubated at 37 °C, then the reaction was initiated by the addition of the substrate. All reactions were carried out in a fluorescence cuvette (Hellma Analytics, Müllheim, Ger-

many), held in the thermostat cell holder of a Jasco FP-8200 fluorescence spectrophotometer (Easton, MD, USA) equipped with a Xe lamp light source. The excitation of the reactions was performed at 360 nm and emission was detected at 450 nm every 10 s for 10 min. All measurements were performed in triplicates. Initial velocities were determined and the reciprocal of initial velocities was plotted against inhibitor concentrations. The inhibitory mode of the compounds on hOGA was assessed by the Cornish–Bowden method, which involves the plotting of $[S]/v_0$ vs. inhibitor concentrations [27]. The linear fitting to the data points resulted in parallel lines referring to competitive inhibition. Inhibition constants (K_i) were determined according to the competitive model of the Dixon method by plotting the reciprocal of initial velocities vs. inhibitor concentrations [28]. The intersection point of the linearly fitted lines gave K_i in nM.

In the case of hHexB inhibition, Michaelis–Menten kinetics were evaluated using *p*NP-GlcNAc as a substrate. The kinetic reactions took place in Eppendorf tubes in a final volume of 400 μ L containing 24 nM HexB, *p*NP-GlcNAc substrate in the range of 0.1–3 mM, and various inhibitor concentrations ranging from 0 to 300 nM in 50 mM citrate-phosphate buffer, pH 5.0. The reactions were incubated at 35 °C and then 50 μ L samples were taken every 60 s. Samples were mixed with a quenching solution of 150 μ L 0.1M Na_2CO_3 and the absorbance of the solutions was measured at 420 nm by a Tecan Sunrise plate reader (Männedorf, Switzerland). All measurements were performed in triplicates. Initial velocities were determined from the data points by linear fit, and then nonlinear regression analyses were performed using the competitive inhibition model to calculate K_i values. GraphPad Prism software was used for the calculations.

3.3. Computational Details

3.3.1. Protein Preparation

hOGA was prepared for Prime protein–ligand refinement calculations using its co-crystallized complex with PUGNAc (PDB code 5UHO; 3.21 Å resolution) and Schrödinger’s Protein Preparation Wizard [21]. Water molecules within 5 Å of the native ligand were initially retained (deleted for subsequent calculations), bond orders were assigned and hydrogen atoms added, with the protonation states for basic/acidic residues based on PROPKA calculated $\text{p}K_a$ ’s at pH 7 [29]. Subsequent optimization of hydroxyl groups, histidine sidechain C/N atom flips and protonation states, and any sidechain O/N atom flips of Gln and Asn residues was based on optimizing hydrogen-bonding networks. The system was finally minimized using OPLS-AA (2005) force field [30] under the constraint of RMSD (heavy atoms) to be maintained within 0.3 Å of the crystallographic atomic positions.

3.3.2. Enzyme–Inhibitor Complex Predictions

Initial models of enzyme–inhibitor complexes for calculations were prepared by mutation of PUGNAc in chain A of the prepared crystallographic complex into the inhibitors **5a–f**. Prime v5.4 enzyme–inhibitor refinements [21] were then performed in the hierarchical optimization mode for each new complex. The default OPLSe force field [31] and the VSGB model of solvation [32] were employed. Residues within 5 Å of PUGNAc in 5UHO were free in all refinement calculations (same 360 atoms), but with hydrogen bond constraints (force constant 100 kcal mol⁻¹ Å⁻²) to the *N*-acetyl-glucosamine moiety to reflect the solved hOGA-PUGNAc crystallographic data; specifically (cf. Table 4), Asp285 carboxylate–inhibitor O4’ and O6’ hydrogens, Gly67 backbone O–ligand O3’ hydrogen, Asp174 and Asp175 sidechain carboxylates–ligand N2’ hydrogen, and Asn280 sidechain -NH₂ with inhibitor acetyl carbonyl O atom. The rest of the protein atoms (beyond 5 Å) were constrained. The number of structures (enzyme–inhibitor models) to return in each case was set to 5. Initial validation of the protocol involved the application of this protocol to the cognate PUGNAc ligand for the reproduction of its solved crystallographic binding mode.

The five output complexes for each inhibitor were then further refined using two methods for comparison: additional Prime v5.4 refinements and QM/MM optimizations.

For the Prime refinements, in this case, the local optimization mode was used, releasing the hydrogen bond constraints used in the initial hierarchical optimization mode calculations. The same protein residues (360 atoms) were free, with the rest of the protein constrained, as before. For the QM/MM optimizations, again the same protein residues were free and constrained as per the Prime calculations; no hydrogen bond constraints were used. In this case, the respective inhibitor was described using QM (QM region) at the M06-2X/6-31+G** level of theory [33–35], and the protein (MM region) was modeled using the OPLS-AA(2005) force field [30]. No cut-offs were used for non-bonded interactions. All QM/MM calculations were performed using QSite (Jaguar v10.2; Impact v81012) [21].

4. Conclusions

A library of 2-acetamido-2-deoxy-D-glucono-1,5-lactone arenesulfonylhydrazones was prepared from D-glucosamine in a five-step synthetic sequence in 26–44% overall yields. These compounds were assayed for their inhibitory activity against human OGA and HexB enzymes by using fluorimetric and spectrophotometric detection, respectively. Both enzymes were inhibited by the sulfonylhydrazones in the nanomolar range, and hence the compounds were considerably potent. However, the selectivity ($K_{i(\text{hHexB})}/K_{i(\text{hOGA})}$) varied from 1.3 to 0.21 to show no significant bias to any of the enzymes. The best inhibitor of hOGA was 2-acetamido-2-deoxy-D-glucono-1,5-lactone 1-naphthalenesulfonylhydrazone with a K_i of 27 nM and this compound had a K_i of 6.8 nM towards hHexB. The possible binding modes of the inhibitors to the hOGA enzyme were analyzed by computational methods (Prime protein–ligand refinement and QM/MM optimizations) to reveal the predicted interactions responsible for the strong binding of the compounds in a preferred *s-cis* conformation along the (C=N)-N(-H;-SO₂) rotatable bond. This study has extended the relatively few structure–activity relationships of OGA inhibitors. However, the nonselective nature of the inhibition towards hHexB necessitates further structural modifications of the glyconolactone sulfonylhydrazone-type inhibitors.

Supplementary Materials: The following are available online at www.mdpi.com/article/10.3390/ijms23031037/s1.

Author Contributions: M.K. synthesized the compounds, recorded routine NMR spectra, carried out the enzyme kinetic measurements, and wrote the paper; I.T. performed the NOE measurements; T.B. designed and supervised the enzymatic measurements; Z.M. and K.S. prepared the recombinant enzymes and participated in the enzyme assays; P.B. supervised and evaluated enzyme kinetics and edited the paper; V.K. supervised the enzyme experiments, raised part of the funding, and edited the paper; J.M.H. performed the computational study and wrote the paper; L.S. conceptualized the research, raised funding, and wrote the paper. All authors have read and agreed to the published version of the manuscript.

Funding: This work received financial support from the Hungarian National Research, Development and Innovation Office (grants 109450, FK-125067, and PD 135034), the EU co-financed by the European Regional Development Fund under the projects GINOP-2.3.2-15-2016-00008 and GINOP-2.3.3-15-2016-00004, the Czech Science Foundation (grant no. 21-01948L to V.K., P.B., K.S., and Z.M.), and COST Action CA18132 GlycoNanoBio (support for a short-term scientific mission to M.K.). I.T. received support from the János Bolyai Research Scholarship of the Hungarian Academy of Sciences (BO/00372/20/7) and the ÚNKP-21-5-DE-471 New National Excellence Program of the Ministry for Innovation and Technology from the source of the National Research, Development and Innovation Fund.

Institutional Review Board Statement: Not applicable.

Informed Consent Statement: Not applicable.

Data Availability Statement: Not applicable.

Acknowledgments: We thank D. Vocadlo (SFU, Burnaby, BC, Canada) for generously providing the gene construct of human OGA.

Conflicts of Interest: The authors declare no conflict of interest.

References

1. Ma, J.; Wu, C.; Hart, G.W. Analytical and Biochemical Perspectives of Protein O-GlcNAcylation. *Chem. Rev.* **2021**, *121*, 1513–1581. <https://doi.org/10.1021/acs.chemrev.0c00884>.
2. Bond, M.R.; Hanover, J.A. O-GlcNAc Cycling: A Link between Metabolism and Chronic Disease. *Annu. Rev. Nutr.* **2013**, *33*, 205–229. <https://doi.org/10.1146/annurev-nutr-071812-161240>.
3. Zachara, E.N. O-GlcNAc a sensor of cellular state: The role of nucleocytoplasmic glycosylation in modulating cellular function in response to nutrition and stress. *Biochim. Biophys. Acta BBA Gen. Subj.* **2004**, *1673*, 13–28. <https://doi.org/10.1016/j.bbagen.2004.03.016>.
4. Hastings, N.B.; Wang, X.; Song, L.; Butts, B.D.; Grotz, D.; Hargreaves, R.; Hess, J.F.; Hong, K.-L.K.; Huang, C.R.-R.; Hyde, L.; et al. Inhibition of O-GlcNAcase leads to elevation of O-GlcNAc tau and reduction of tauopathy and cerebrospinal fluid tau in rTg4510 mice. *Mol. Neurodegener.* **2017**, *12*, 1–16. <https://doi.org/10.1186/s13024-017-0181-0>.
5. Zhu, Y.; Shan, X.; Yuzwa, S.A.; Vocadlo, D.J. The Emerging Link between O-GlcNAc and Alzheimer Disease. *J. Biol. Chem.* **2014**, *289*, 34472–34481. <https://doi.org/10.1074/jbc.r114.601351>.
6. Yu, Y.; Zhang, L.; Li, X.; Run, X.; Liang, Z.; Li, Y.; Liu, Y.; Lee, M.H.; Grundke-Iqbal, I.; Iqbal, K.; et al. Differential Effects of an O-GlcNAcase Inhibitor on Tau Phosphorylation. *PLoS ONE* **2012**, *7*, e35277. <https://doi.org/10.1371/journal.pone.0035277>.
7. Yuzwa, A.S.; Shan, X.; Macauley, M.S.; Clark, T.; Skorobogatko, Y.; Vosseller, K.; Vocadlo, D.J. Increasing O-GlcNAc slows neurodegeneration and stabilizes tau against aggregation. *Nat. Chem. Biol.* **2012**, *8*, 393–399. <https://doi.org/10.1038/nchembio.797>.
8. Dong, D.; Hart, G. Purification and characterization of an O-GlcNAc selective N-acetyl- β -D-glucosaminidase from rat spleen cytosol. *J. Biol. Chem.* **1994**, *269*, 19321–19330. [https://doi.org/10.1016/s0021-9258\(17\)32170-1](https://doi.org/10.1016/s0021-9258(17)32170-1).
9. Hattie, M.; Cekic, N.; Debowski, A.W.; Vocadlo, D.J.; Stubbs, K.A. Modifying the phenyl group of PUGNAc: Reactivity tuning to deliver selective inhibitors for N-acetyl-D-glucosaminidases. *Org. Biomol. Chem.* **2016**, *14*, 3193–3197. <https://doi.org/10.1039/c6ob00297h>.
10. Macauley, M.; Whitworth, G.E.; Debowski, A.W.; Chin, D.; Vocadlo, D. O-GlcNAcase Uses Substrate-assisted Catalysis: Kinetic analysis and development of highly selective mechanism-inspired inhibitors. *J. Biol. Chem.* **2005**, *280*, 25313–25322. <https://doi.org/10.1074/jbc.m413819200>.
11. Macauley, M.S.; Vocadlo, D.J. Increasing O-GlcNAc levels: An overview of small-molecule inhibitors of O-GlcNAcase. *Biochim. et Biophys. Acta BBA Gen. Subj.* **2010**, *1800*, 107–121. <https://doi.org/10.1016/j.bbagen.2009.07.028>.
12. Kiss, M.; Szabó, E.; Bocska, B.; Sinh, L.T.; Fernandes, C.P.; Timári, I.; Hayes, J.M.; Somsák, L.; Barna, T. Nanomolar inhibition of human OGA by 2-acetamido-2-deoxy-D-glucono-1,5-lactone semicarbazone derivatives. *Eur. J. Med. Chem.* **2021**, *223*, 113649. <https://doi.org/10.1016/j.ejmech.2021.113649>.
13. Mangholz, S.E.; Vasella, A. Glycosylidene Carbenes. Part 5. Synthesis of Glycono-1,5-lactone Tosylhydrazones as Precursors of Glycosylidene Carbenes. *Helv. Chim. Acta* **1991**, *74*, 2100–2111. <https://doi.org/10.1002/hlca.19910740845>.
14. Mangholz, S.E.; Briner, K.; Bernet, B.; Vasella, A. Glycosylidene Carbenes. Part 32. *Helv. Chim. Acta* **2003**, *86*, 2490–2508. <https://doi.org/10.1002/hlca.200390202>.
15. Somsák, L.; Praly, J.-P.; Descotes, G. Sodium Salt of D-Glucono-1,5-lactone Tosylhydrazone: A Ready Access to a New Glucosylidene Carbene Precursor. *Synlett* **1992**, *1992*, 119–120. <https://doi.org/10.1055/s-1992-21284>.
16. Chaplin, D.; Crout, D.H.G.; Bornemann, S.; Hutchinson, D.W.; Khan, R. Conversion of 2-acetamido-2-deoxy- β -D-glucopyranose (N-acetylglucosamine) into 2-acetamido-2-deoxy- β -D-galactopyranose (N-acetylgalactosamine) using a biotransformation to generate a selectively deprotected substrate for S_N2 inversion. *J. Chem. Soc. Perkin Trans.* **1992**, *1*, 235–237. <https://doi.org/10.1039/p19920000235>.
17. Kartha, K.R.; Mukhopadhyay, B.; Field, R. Practical de-O-acylation reactions promoted by molecular sieves. *Carbohydr. Res.* **2004**, *339*, 729–732. <https://doi.org/10.1016/j.carres.2003.11.021>.
18. Zhang, G.; Fan, Q.; Wang, H.; Zhao, Y.; Ding, C. NaHSO₃-Mediated Direct Synthesis of Sulfinic Esters from Sulfonyl Hydrazides under Transition-Metal-Free Conditions. *Adv. Synth. Catal.* **2021**, *363*, 833–837. <https://doi.org/10.1002/adsc.202001202>.
19. Thiele, C.M.; Petzold, K.; Schleucher, J. Easy Roesy: Reliable Cross-Peak Integration in Adiabatic Symmetrized ROESY. *Chem. Eur. J.* **2009**, *15*, 585–588. <https://doi.org/10.1002/chem.200802027>.
20. Krejzová, J.; Kulik, N.; Slámová, K.; Křen, V. Expression of human β -N-acetylhexosaminidase B in yeast eases the search for selective inhibitors. *Enzym. Microb. Technol.* **2016**, *89*, 1–6. <https://doi.org/10.1016/j.enzmictec.2016.03.003>.
21. *Schrödinger Release 2018-4*; Schrödinger, LLC: New York, NY, USA, 2018.
22. Manta, S.; Xipnitou, A.; Kiritsis, C.; Kantsadi, A.L.; Hayes, J.M.; Skamnakis, V.T.; Lamprakis, C.; Kontou, M.; Zoumpoulakis, P.; Zographos, S.E.; et al. 3'-Axial CH₂OH Substitution on Glucopyranose does not Increase Glycogen Phosphorylase Inhibitory Potency. QM/MM-PBSA Calculations Suggest Why. *Chem. Biol. Drug Des.* **2012**, *79*, 663–673. <https://doi.org/10.1111/j.1747-0285.2012.01349.x>.
23. Murphy, R.B.; Philipp, D.M.; Friesner, R.A. A mixed quantum mechanics/molecular mechanics (QM/MM) method for large-scale modeling of chemistry in protein environments. *J. Comput. Chem.* **2000**, *21*, 1442–1457. [https://doi.org/10.1002/1096-987x\(200012\)21:163.0.co;2-o](https://doi.org/10.1002/1096-987x(200012)21:163.0.co;2-o).
24. Lin, F.-Y.; MacKerell, J.A.D. Do Halogen–Hydrogen Bond Donor Interactions Dominate the Favorable Contribution of Halogens to Ligand–Protein Binding? *J. Phys. Chem. B* **2017**, *121*, 6813–6821. <https://doi.org/10.1021/acs.jpcc.7b04198>.

25. Zhao, Y.; Li, J.; Gu, H.; Wei, N.; Xu, Y.-C.; Fu, W.; Yu, Z. Conformational Preferences of π - π Stacking Between Ligand and Protein, Analysis Derived from Crystal Structure Data Geometric Preference of π - π Interaction. *Interdiscip. Sci. Comput. Life Sci.* **2015**, *7*, 211–220. <https://doi.org/10.1007/s12539-015-0263-z>.
26. Gyöngyösi, T.; Timári, I.; Sinnaeve, D.; Luy, B.; Kövér, K.E. Expedited Nuclear Magnetic Resonance Assignment of Small- to Medium-Sized Molecules with Improved HSQC–CLIP–COSY Experiments. *Anal. Chem.* **2021**, *93*, 3096–3102. <https://doi.org/10.1021/acs.analchem.0c04124>.
27. Cornish-Bowden, A. A simple graphical method for determining the inhibition constants of mixed, uncompetitive and non-competitive inhibitors (Short Communication). *Biochem. J.* **1974**, *137*, 143–144. <https://doi.org/10.1042/bj1370143>.
28. Dixon, M. The determination of enzyme inhibitor constants. *Biochem. J.* **1953**, *55*, 170–171. <https://doi.org/10.1042/bj0550170>.
29. Søndergaard, C.R.; Olsson, M.H.M.; Rostkowski, M.; Jensen, J.H. Improved Treatment of Ligands and Coupling Effects in Empirical Calculation and Rationalization of pK_a Values. *J. Chem. Theory Comput.* **2011**, *7*, 2284–2295. <https://doi.org/10.1021/ct200133y>.
30. Kaminski, G.A.; Friesner, R.A.; Tirado-Rives, J.; Jorgensen, W.L. Evaluation and Reparametrization of the OPLS-AA Force Field for Proteins via Comparison with Accurate Quantum Chemical Calculations on Peptides. *J. Phys. Chem. B* **2001**, *105*, 6474–6487. <https://doi.org/10.1021/jp003919d>.
31. Harder, E.; Damm, W.; Maple, J.; Wu, C.; Reboul, M.; Xiang, J.Y.; Wang, L.; Lupyan, D.; Dahlgren, M.K.; Knight, J.L.; et al. OPLS3: A Force Field Providing Broad Coverage of Drug-like Small Molecules and Proteins. *J. Chem. Theory Comput.* **2016**, *12*, 281–296. <https://doi.org/10.1021/acs.jctc.5b00864>.
32. Li, J.; Abel, R.; Zhu, K.; Cao, Y.; Zhao, S.; Friesner, R.A. The VSGB 2.0 model: A next generation energy model for high resolution protein structure modeling. *Proteins Struct. Funct. Bioinform.* **2011**, *79*, 2794–2812. <https://doi.org/10.1002/prot.23106>.
33. Zhao, Y.; Truhlar, D.G. The M06 suite of density functionals for main group thermochemistry, thermochemical kinetics, non-covalent interactions, excited states, and transition elements: Two new functionals and systematic testing of four M06-class functionals and 12 other functionals. *Theor. Chem. Acc.* **2008**, *120*, 215–241. <https://doi.org/10.1007/s00214-007-0310-x>.
34. Francl, M.; Pietro, W.J.; Hehre, W.J.; Binkley, J.S.; Gordon, M.S.; DeFrees, D.J.; Pople, J.A. Self-consistent molecular orbital methods. XXIII. A polarization-type basis set for second-row elements. *J. Chem. Phys.* **1982**, *77*, 3654–3665. <https://doi.org/10.1063/1.444267>.
35. Hehre, W.J.; Ditchfield, R.; Pople, J.A. Self-Consistent Molecular Orbital Methods. XII. Further Extensions of Gaussian-Type Basis Sets for Use in Molecular Orbital Studies of Organic Molecules. *J. Chem. Phys.* **1972**, *56*, 2257–2261. <https://doi.org/10.1063/1.1677527>.